Structural and Spectroscopical Characterization of μ-oxo Bridged Iron(III) Bromide Complexes of Pyclen Ligands

Nicola Panza,[a*] Armando di Biase,[a] and Alessandro Caselli[a]

[a]Department of Chemistry, Università degli Studi di Milano and CNR-SCITEC, via Golgi 19, 20133 Milano, Italy. E-mail: nicola.panza@unimi.it; phone: +39 02 50314372.

ARTICLE INFO

Keywords:

Iron; μ-oxo; Raman spectroscopy; Pyclen; Macrocyclic Ligands.

ABSTRACT:

Binuclear iron oxo-bridged complexes have found much interest since the early 80's as synthetic models for relevant biological molecules, catalysts and magnetic probes. In this work, a series of iron(III)bromide-based oxo-bridged complexes of Pyclen ligands was prepared, with the aim of investigating the peculiar iron-oxygen bond features in different molecular environments. We observed the influence of the steric hindrance of the ligands employed in this study towards the formation of symmetrical and non-symmetrical *μ-oxo* complexes, and we confirmed this peculiar behaviour by single crystal X-ray diffraction and Raman spectroscopy. We report here structural and spectroscopical insight of three unprecedented oxo-iron complexes and their relative precursors, enlarging the existing database of these particular class of metal complexes.

1. Introduction

The synthesis and characterization of iron(III) oxo-bridged complexes have been a topic of interest in the field of biomolecular catalysis and modelling since the early 80's, where the focus was on the investigation of the reactivity of enzymes such as Hemerythrin and Oxyhemerythrin [1–6]. Another aspect of interest of this peculiar class of iron(III) molecules was related to their magnetic properties, where strong antiferromagnetic coupling was spectroscopically investigated on synthetic model compounds, based on both *heme* and non-*heme* complexes [7–10]. Oxygen-bridging complexes of different ligands were also suggested as existing species in certain catalytic cycles, but nonetheless, they

were pointed out as both proper catalytically active species [11–14], reactive intermediates [15,16] or dead-end species [17]. The difficulty in predicting the nature of the truly active catalyst and the possible intermediates is still a limiting factor in iron oxidation catalysis. In our group, we are fully involved in the synthesis of macrocyclic ligands of the Pyclen family (Pyclen = 3,6,9-triaza-1(2,6)-pyridinacyclodecaphane) [18–25]. Their tetra-aza macrocyclic core is well-known to be a suitable coordination site for different transition metals, in different oxidation states [26,27]. Studies of Pyclen type iron complexes have been reported [28,29], highlighting the role of high valent oxo-species in catalytic oxidations [30–33]. In a very recent paper, K. Green and co-workers reported the isolation and characterization of iron(III) oxo-bridged Pyclen complexes as intermediates in the C-C coupling of pyrrole and phenylboronic acid and proved their negligible catalytic activity with respect to their monomeric counterparts [17]. These compounds were obtained by the interaction of mononuclear iron species with a base in the presence of water. A related mononuclear iron(III) complex [34] was already prepared using iron(III) bromide and used as catalyst by our research group and for this reason, inspired by this new findings we synthetised and characterized three novel symmetric and non-symmetric iron(III) bromide oxo-bridged Pyclen complexes with different coordination environment. The crystal structures were obtained by X-Ray diffraction and Fe-O-Fe vibrational bands were assigned by solid-state Raman spectroscopy, which can be used as an intuitive and useful tool to investigate reactive species in iron-based catalysis.

2. Results

This works, as often happens in scientific research, comes from a serendipitous finding. While attempting the synthesis of a well-defined iron(III) complex of sterically hindered Pyclen ligand **L1** (Figure 1), as described in a previous paper [35], in fact, we obtained an unexpected result. It turned out that the strong basicity of this ligand led to its protonation in the reaction media, and the treatment with iron(III) bromide, instead of the coordination of the metal ion into the macrocyclic skeleton, yielded to the ferrate salt **1** (Figure 2), which still proved to be a competent catalyst for CO_2 coupling with epoxides. When we tried to neutralize the ligand in situ prior to the addition of iron(III) bromide, we ended up obtaining an unclear mixture of different compounds.

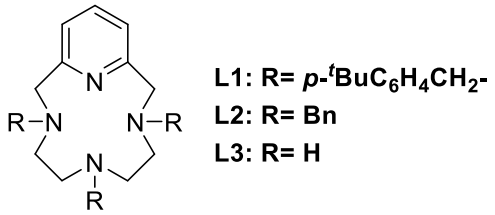

Figure 1. Structure of the Pyclen derivatives **L1**-**L3** used as ligands in this work (Bn = benzyl).

On the other hand, following a procedure reported in the literature [17] to obtain specific iron(III) chloride oxo-bridged complexes, by reaction of the mononuclear precursors and triethylamine in acetonitrile and water, we were able to obtain and characterize three new iron(III) bromide μ-oxo compounds. In our case, the addition of water was proved to not be mandatory when using non-distilled solvents. The influence of the different coordination environment on the formation of oxygen bridged species was investigated by changing the steric hindrance around the macrocyclic core (Figure 1).

2.1 Synthesis and structural determination

2.1.1 [(L1FeBr)μ-O(FeBr$_3$)] (2)

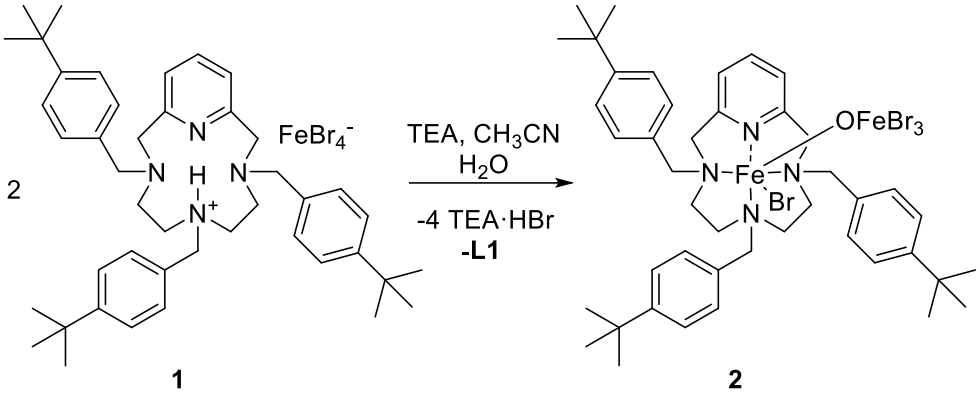

Scheme 1. Synthesis of complex**2** from compound **1**.

Ligand **L1** and the ferrate salt **1** were synthetized as previously reported [35]. After dissolution of **1** in acetonitrile, triethylamine was diluted in acetonitrile and added dropwise (Scheme 1). Slow diffusion of diethyl ether in the acetonitrile solution led to the formation of red block shaped crystals after several weeks. Crystal structure of the novel compound **2** was obtained by X-Ray diffraction at 150 K. The reaction proceeds with the loss of a ligand **L1** molecule to yield a non-symmetrical di-iron(III) complex. It is likely that the steric bulkiness of **L1** disfavoured the approaching of two identical units. To account for the observed stoichiometry, the bridging μ-oxo atom is furnished by adventitious water (the reaction is performed in air and with non-distilled wet solvents) and 4 equivalent of triethyl ammonium bromide are released. Complex **2** crystallizes in the triclinic crystal system, s.g. $P\bar{1}$ (Table 1). The asymmetric

unit comprises one molecule of **2** along with disordered acetamide molecules, formed by basic hydrolysis of acetonitrile. As shown in **Figure 2**, the complex has a dimeric nature with two iron atoms in different coordination environments. The overall coordination geometry is similar to that of already reported complexes with a $N_4XFe(\mu\text{-oxo})FeX_3$ core [11,12,14,36–39]: **Fe1** is hexacoordinated in a distorted octahedral geometry by the four nitrogen donors of the tetraaza-macrocycle, a bromine atom and a μ-oxo ligand; this μ-oxo bridge connects **Fe1** to the tetrahedral iron centre **Fe2**, surrounded by three bromine atoms and the linking oxygen atom. The **Fe1-O-Fe2** fragment is bent, with an angle of 153.1(2)° and a Fe···Fe distance of 3.4398(9) Å. The macrocycle is folded in a *cis*-(+++) conformation with the N substituents that are positioned above the N4 macrocyclic plane [34,40]. However, the structure of the macrocyclic ligand in complex **2** differs greatly from that of the related hydrobromide salt of **L1** [35]. In fact, when the ligand is protonated, the bonds between the substituted nitrogen atoms and the corresponding pendants are rotated in such a way that the bulky substituents hinder the macrocyclic cavity. In the case of **2**, instead, the substituents are pointing away from the macrocyclic cavity, allowing the host of an iron(III) cation.

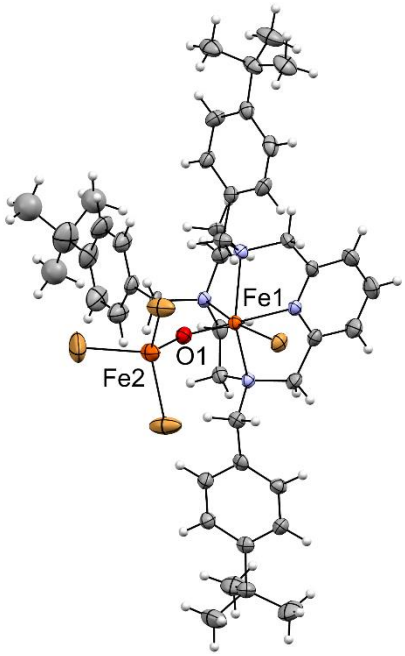

Figure 2. Structure of **2** with thermal ellipsoid at 50 % probability level: Solvent molecules are omitted for clarity and disordered moieties are treated with isotropic models (details in Supporting Information). Selected bond distances (Å): Fe1-O1 1.788(4), Fe2-O1 1.749(4).

2.1.2 [(L2FeBr)μ-O(FeBr$_2$)μ-O(L2FeBr)]Br (4)

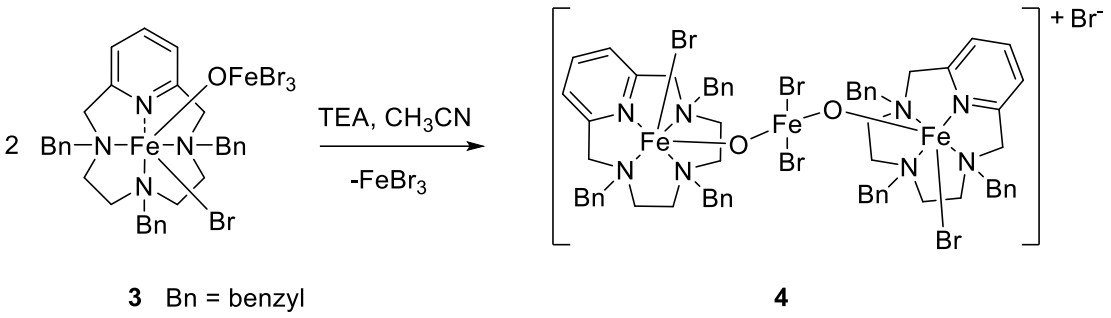

Scheme 2. Synthesis of complex **4** from compound **3**.

We next studied the coordination behavior of the benzyl substituted Pyclen ligand **L2**. In analogy to what observed for ligand **L1**, also in this case, the addition of excess of iron(III) bromide (2 eqivalents with respect to the ligand) under wet conditions in acetonitrile yielded to the isolation of complex **3** [41], whose structure is depicted in Scheme 2, based on the close analogy of its analytical (Elemental Analysis) and spectroscopic characterization (Raman spectroscopy, *vide infra*). Further treatment of **3** with a base (TEA) led to the formation of an unexpected very interesting trinuclear iron(III) species, complex **4**. The lesser steric hindrance of **L2** in comparison with **L1** and the presence of a bridging iron unit allows in this case for the formation of this trimer with two iron Pyclen moieties bridged by a tetrahedral ferrate anion. Red prismatic crystals of **4** were obtained by slow diffusion of diethyl ether in a solution of acetonitrile/MeOH. Compound **4** crystallizes in the orthorhombic crystal system, s.g. $Pca2_1$ (Table1). The asymmetric unit contains one molecule of **4** along with a bromide counterion plus disordered molecules of acetonitrile and methanol. The crystal structure is displayed in **Figure 3**. Two octahedral iron centers, **Fe1** and **Fe3**, interact each with four nitrogen donors of the tetraaza-macrocycle, a bromide ligand and the μ-O atoms and they are connected by a bridging tetrahedral **FeBr$_2$O$_2$** unit *via* μ-oxo linkages. Fe-O-Fe angles are 173.3(3)° for Fe1-O1-Fe2 and 173.4(3)° for Fe3-O2-Fe2, while Fe···Fe distances are 3.5290(4) Å for Fe1···Fe2 and 3.5470(3) Å for Fe3···Fe2. Moreover, the octahedral fragments are positioned in such a way that the two bromide ligands point in opposite direction to each other. Again, the macrocycles are folded in *cis*-(+++) conformation [40], with the bulky *N*-benzyl substituents that point above the N4 macrocyclic plane and leave the macrocyclic cavity available for the coordination to the iron atoms. It is worth mentioning that an analogous species with a higher nuclearity was obtained by Brewer and co-workers [17]. In the presence of a less hindered tetraaza-macrocycle, they crystallized a tetranuclear complex in which three octahedral iron(III) units are connected by a tetrahedral iron(III) centre.

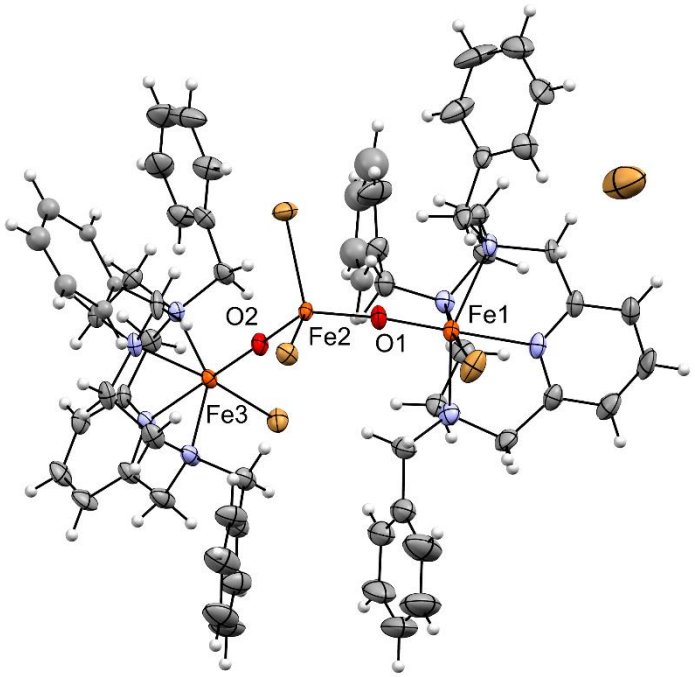

Figure 3. Structure of **3** with thermal ellipsoid at 50 % probability level: Solvent molecules are omitted for clarity and disordered moieties are treated with isotropic models (details in Supporting Information). Selected bond distances (Å): Fe1-O1 1.764(4), Fe3-O2 1.766(4), Fe2-O1 1.770(4), Fe2-O2 1.786(4).

2.1.3 [μ-O(L3FeBr)$_2$]Br$_2$ (6)

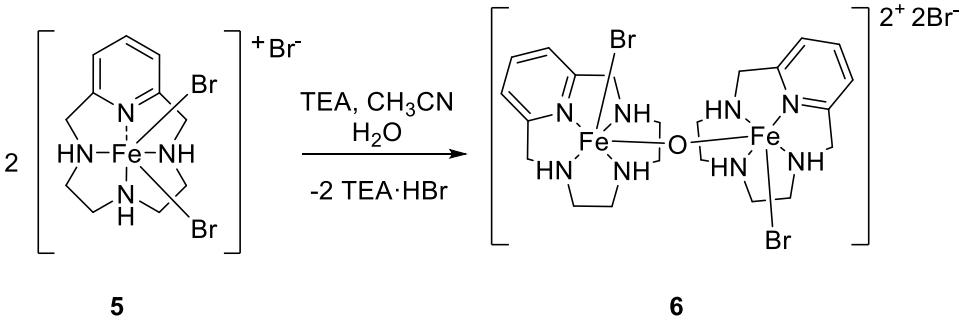

5 **6**

Scheme 3. Synthesis of complex **6** from the monomeric complex **5**.

Complex **5** was already reported as catalyst for the selective oxidation of alcohols to aldehydes by our research group and the corresponding iron(III) complex with chloride anions was found to be a competent catalyst for C-C coupling of boronic acids and pyrrole [17]. In the same fashion of the previously described syntheses of complexes **2** and **4**, treatment of **5** with triethylamine in wet acetonitrile led to the formation of compound **6**, which has its chloride counterpart counterion the complexes reported by Green [17]. In this case no steric hindrance is present in **L3** and this permits two macrocyclic units to approach

and bridge by an oxygen atom to form a highly symmetric compound. Black polyhedric crystals of **6** suitable for X-ray diffraction were grown by slow diffusion of diethyl ether in a solution of acetonitrile/MeOH. Complex **6** crystallizes in the monoclinic crystal system, s.g. $C2/m$ (Table 1) The asymmetric unit consists of only one half of the **O-FeL3Br** moiety and a bromide anion in the second coordination sphere. **6** features two identical iron centres (**Figure 4**). Both iron atoms are 6-fold coordinated in a distorted octahedral geometry by the linking oxygen, a bromide ligand and the tetraaza-macrocycle **L3**, which adopts its usual *cis*-(+++) conformation [34, 40]. The complex is di-cationic and two bromide anions are required for charge balance. The oxygen atom lies on an inversion centre so that the two **O-FeL3Br** units are symmetrical and placed in a staggered conformation. Furthermore, the **Fe-O-Fe** fragment is linear with an angle of 180° and a Fe···Fe separation of 3.5360(5) Å. As previously mentioned, the structure of **6** resembles that of **[L3ClFe-O-FeL3Cl]**$^{2+}$ obtained by Green and co-workers in two different crystal forms [17], even though in those cases the Fe-O-Fe unit was slightly bent. A search in the CSD revealed that the XFe-O-FeX motif with a linear μ-oxo bridge and a staggered conformation of the halide donors also appears in numerous complexes of tetraaza-macrocyclic or chelating ligands [16,42–50]. Table 1 summarizes the crystal data for complexes **2**, **4** and **6**.

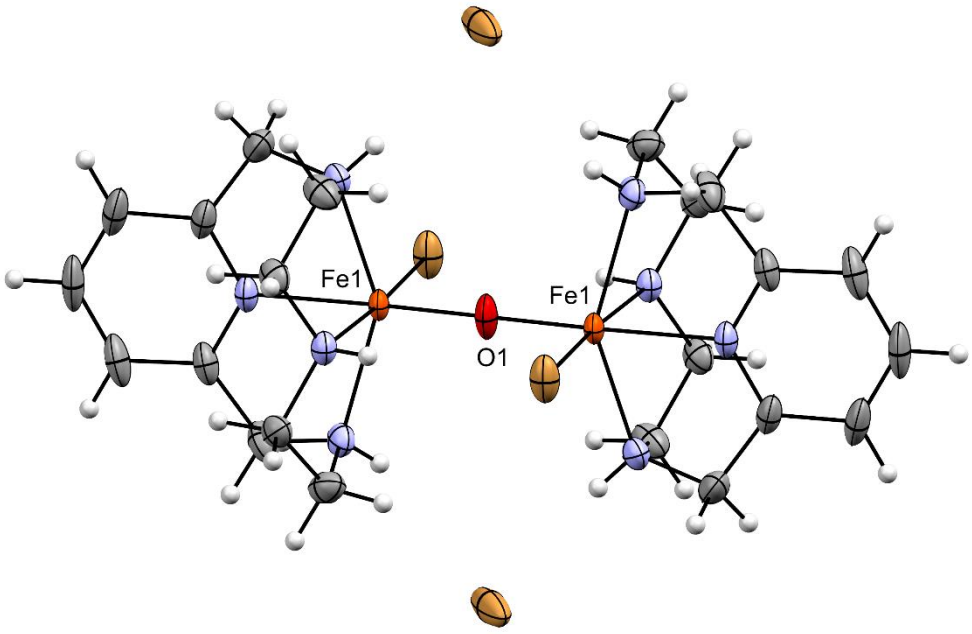

Figure 4. Structure of **6** with thermal ellipsoid at 50 % probability level: Solvent molecules are omitted for clarity (details in Supporting Information). Selected bond distances (Å): Fe1-O1 1.7680(4) (the two iron atoms are symmetry related by -x+1,-y,-z+1).

Table 1. Crystal data and structure refinement

Identification code	**2**	**4**	**6**
Empirical formula	$(C_{44}H_{60}Br_4Fe_2N_4O)\cdot 1.35(CH_3CONH_2)\cdot 0.6(CH_3CN)$	$(C_{64}H_{72}Br_5Fe_3N_8O_2)\cdot 1.5(CH_3CN)\cdot 2(CH_3OH)$	$(C_{22}H_{36}Br_4Fe_2N_8O)\cdot 3(CH_3OH)$
Formula weight (g mol^{-1})	1188.06	1676.04	943.96
Temperature (K)	150(2)	150(2)	150(2)
Wavelength (Å)	0.71073	0.71073	0.71073
Crystal system	Triclinic	Orthorhombic	Monoclinic
Space group	$P\bar{1}$	$Pca2_1$	$C2/m$
Unit cell dimensions			
a (Å)	9.745(3)	22.073(2)	12.414(1)
b (Å)	15.884(6)	13.646(2)	17.616(1)
c (Å)	19.997(7)	24.473(3)	8.5625(7)
α (°)	78.260(4)	90	90
β (°)	76.346(4)	90	109.113(1)
γ (°)	72.282(4)	90	90
Volume ($Å^3$)	2836(3)	7371(2)	1769.3(4)
Z	2	4	2
Calculated density (Mg m^{-3})	1.391	1.510	1.772
Absorption coefficient (mm^{-1})	3.368	3.344	5.379
F(000)	1200	3392	932
Crystal size (mm^3)	0.283 x 0.126 x 0.121	0.353 x 0.306 x 0.102	0.332 x 0.297 x 0.203
Theta range for data collection (°)	1.360 to 24.860	1.492 to 28.759	2.086 to 28.433
Index ranges	$-11 \le h \le 11$, $-18 \le k \le 18$, $-23 \le l \le 23$	$-29 \le h \le 29$, $-18 \le k \le 18$, $-33 \le l \le 33$	$-16 \le h \le 16$, $-23 \le k \le 23$, $-11 \le l \le 11$
Reflections collected	18530	67187	8126
Independent reflections	9739 [$R_{(int)} = 0.0638$]	19058 [$R_{(int)} = 0.0390$]	2301 [$R_{(int)} = 0.0145$]
Max. and min. transmission	0.7449 and 0.5207	0.7458 and 0.5648	0.7454 and 0.5636
Refinement method	Full-matrix least-squares on F^2	Full-matrix least-squares on F^2	Full-matrix least-squares on F^2
Data / restraints / parameters	9739 / 28 / 550	19058 / 12 / 786	2301 / 3 / 115
Goodness-of-fit on F^2	0.988	1.07	1.059
Final R indices [I>2sigma(I)]	$R_1 = 0.0563$, $wR_2 = 0.1443$	$R_1 = 0.0451$, $wR_2 = 0.1033$	$R_1 = 0.0293$, $wR_2 = 0.0748$
R indices (all data)	$R_1 = 0.1023$, $wR_2 = 0.1622$	$R_1 = 0.0585$, $wR_2 = 0.1094$	$R_1 = 0.0319$, $wR_2 = 0.0762$
Largest diff. peak and hole (e $Å^{-3}$)	1.138 and -1.355	1.820 and -1.627	1.134 and -0.930
CCDC deposition number	2175110	2175109	2175108

2.2 Raman spectroscopy

Raman spectroscopy is a widely employed analytical technique for the study of the vibrational bands associated to the Fe-O-Fe fragment in proteins and model compounds [4,6,7,51,52]. Even in our case, Raman spectroscopy turned to be a fundamental tool to characterize the μ-oxo complexes under investigation.

We performed our analysis using an excitation wavelength of 532 nm and collecting the backscattering light from the powdered samples (details in the experimental section). The relevant observed Raman bands are listed in Table 2.

2.2.1 [L1FeBr)μ-O(FeBr$_3$)] (2)

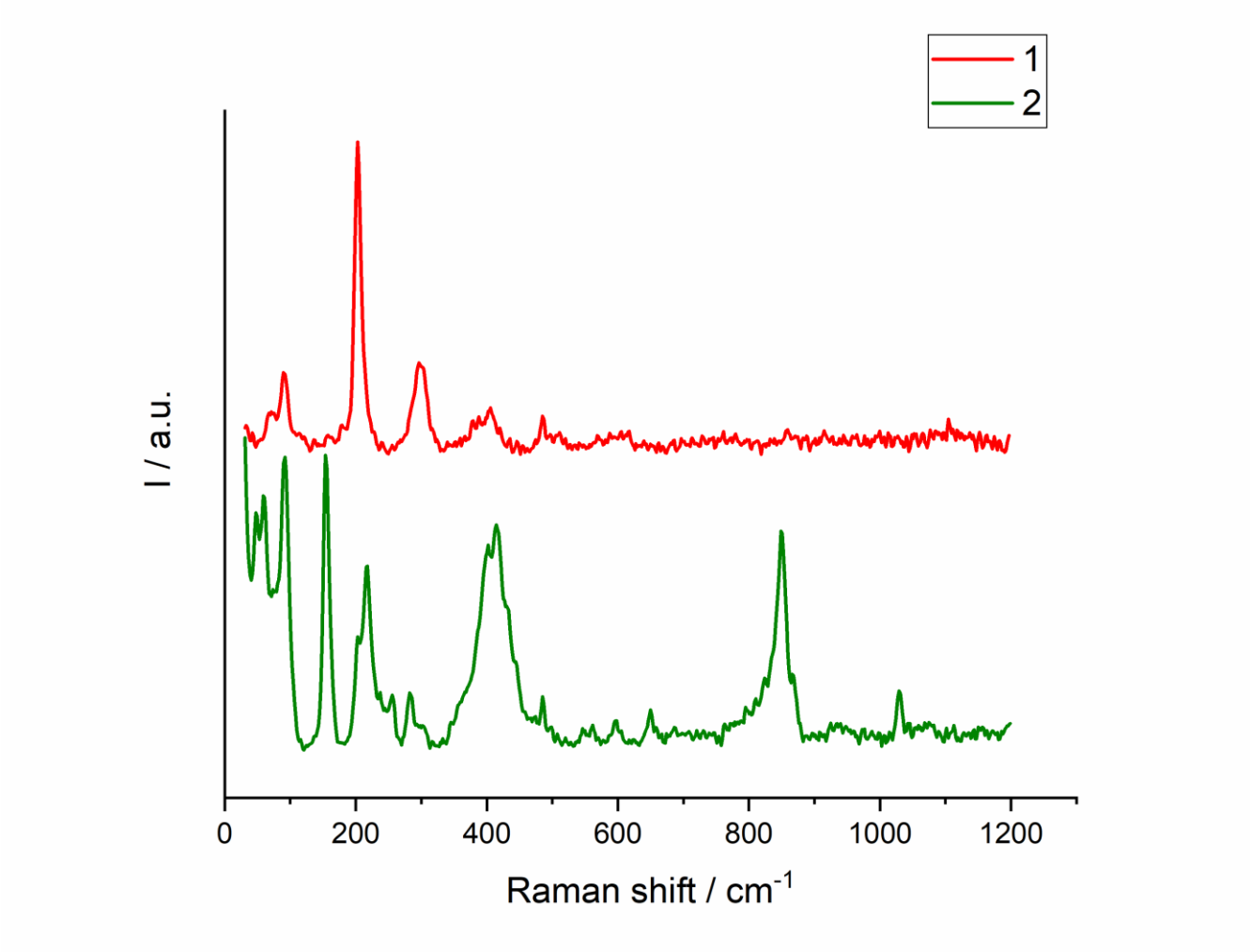

Figure 5. Raman spectra of precursor **1** (top red line, 1) and of dimeric complex **2** (bottom green line, 2).

The Raman spectra of the starting complex **1** is a direct proof of the presence of a **$FeBr_4^-$** anion. The most intense lines at **203 cm^{-1}** and **294 cm^{-1}** can indeed be assigned as **A_1** and **T_2** vibrational bands of the aforementioned tetrahedral unit [53] and the less intense one at ~**90 cm^{-1}** tentatively assigned as the **E** mode [54]. As a proof of the formation of the oxo-bridged complex, the Raman spectra of **2** clearly shows the presence of two intense bands at **414 cm^{-1}** and **849 cm^{-1}**, which can be respectively assigned to the symmetric (ν_s) and asymmetric (ν_{as})**Fe-O-Fe** vibrations [4,7,52]. In analogy with related μ-oxo complexes of Ru and Os [55], the sharp line at ~ 154 cm^{-1} might be assigned to the Fe-O-Fe bending vibration (δ), even though this mode was associated to a line at ~ 210 cm^{-1} in the $[Cl_3Fe\text{-}O\text{-}FeCl_3]^{2-}$

dianion [56]. The formation of complex **2** also resulted in the modification of the whole spectra in the region between **200-300 cm**$^{-1}$, a region where Fe-Br stretching bands are usually observed [57–59], due to a lowering of the overall symmetry by the formation of a $N_4BrFe(O)FeBr_3$ unit.

2.2.2 [(L2FeBr)μ-O(FeBr$_2$)μ-O(L2FeBr)]Br (4)

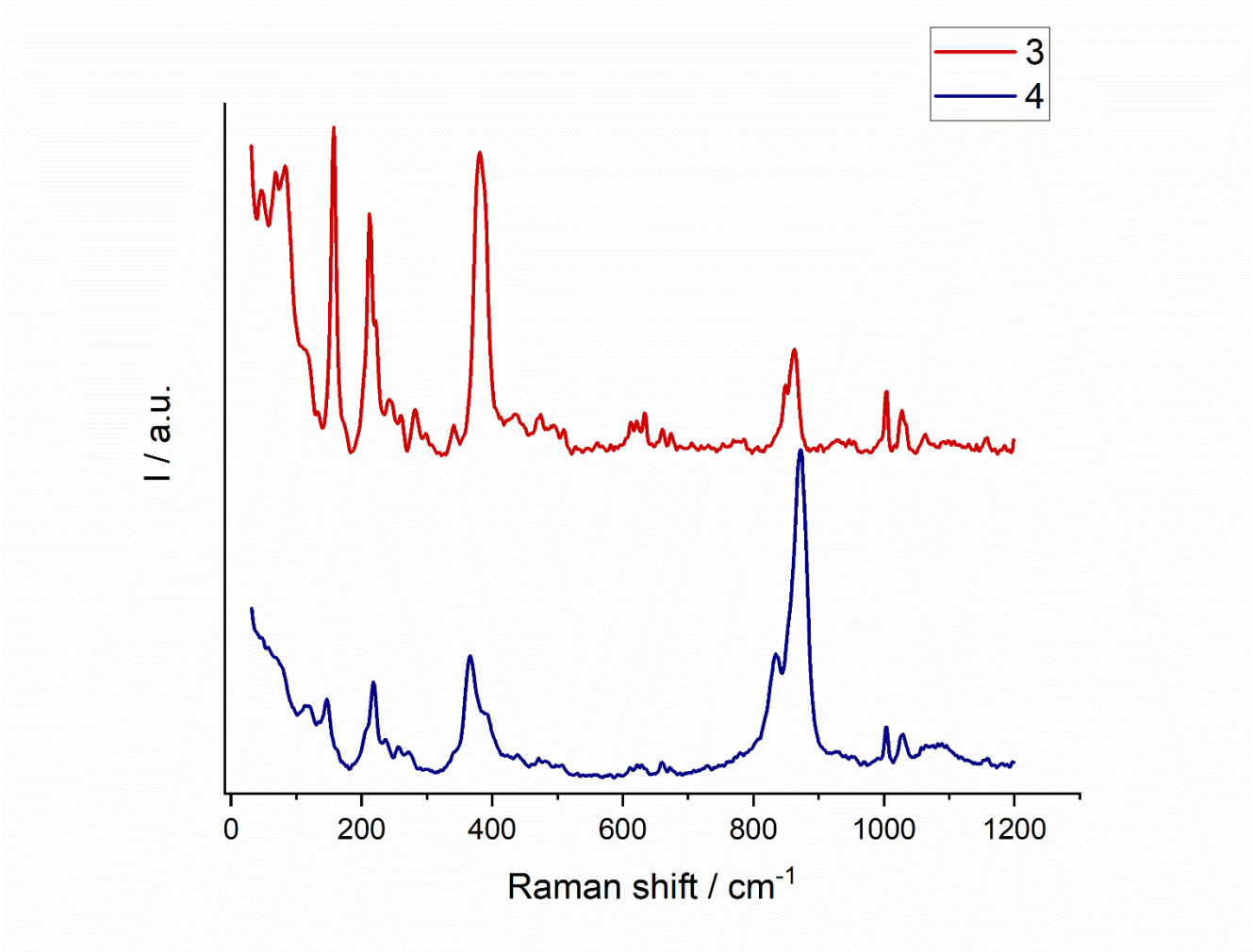

Figure 6. Raman spectra of compound **3** (top red line, 3) and of trimeric complex **4** (bottom blue line, 4).

At the very beginning, the structure of the precursor **3** was only assigned by Elemental Analysis and Mass Spectroscopy. It must be noted that for the ESI-MS experiments, the ionization of complexes **2**, **4** and **6** in methanol resulted in the formation of putative [**L1**-**3**Fe(OMe)] fragments (see experimental) which are indeed not useful in the determination of the molecular structure but rather a mere confirmation of the successful iron coordination in the macrocyclic ligands. All the attempts to crystallize the starting complex **3** failed and for this reason Raman Spectroscopy proved to be a fundamental tool to elucidate its true nature. In fact, as shown in Figure 6, the spectra of **3** closely resemble that of complex **2** (see figure S4). On these bases, we were able to claim the presence of two non-symmetric iron units bridged

by an oxygen atom, with ν_s at **378 cm^{-1}** and ν_{as} at **861 cm^{-1}**. The reaction of **3** with a base afforded compound **4** in which two identical octahedral coordinated iron units are connected to an unusual tetrahedral **FeO_2Br_2** fragment *via* μ-oxo bridges. As we can see in figure 6, the Raman spectra of **4** and the precursor share to a large extent the same features, but with inverted intensities of ν_s and ν_{as} modes. An increasing asymmetry of the two iron centers involved in the vibration has been invoked to account for the enhancement of ν_{as} [4,5,60].

2.2.3 [μ-O(L3FeBr)$_2$]Br$_2$ (6)

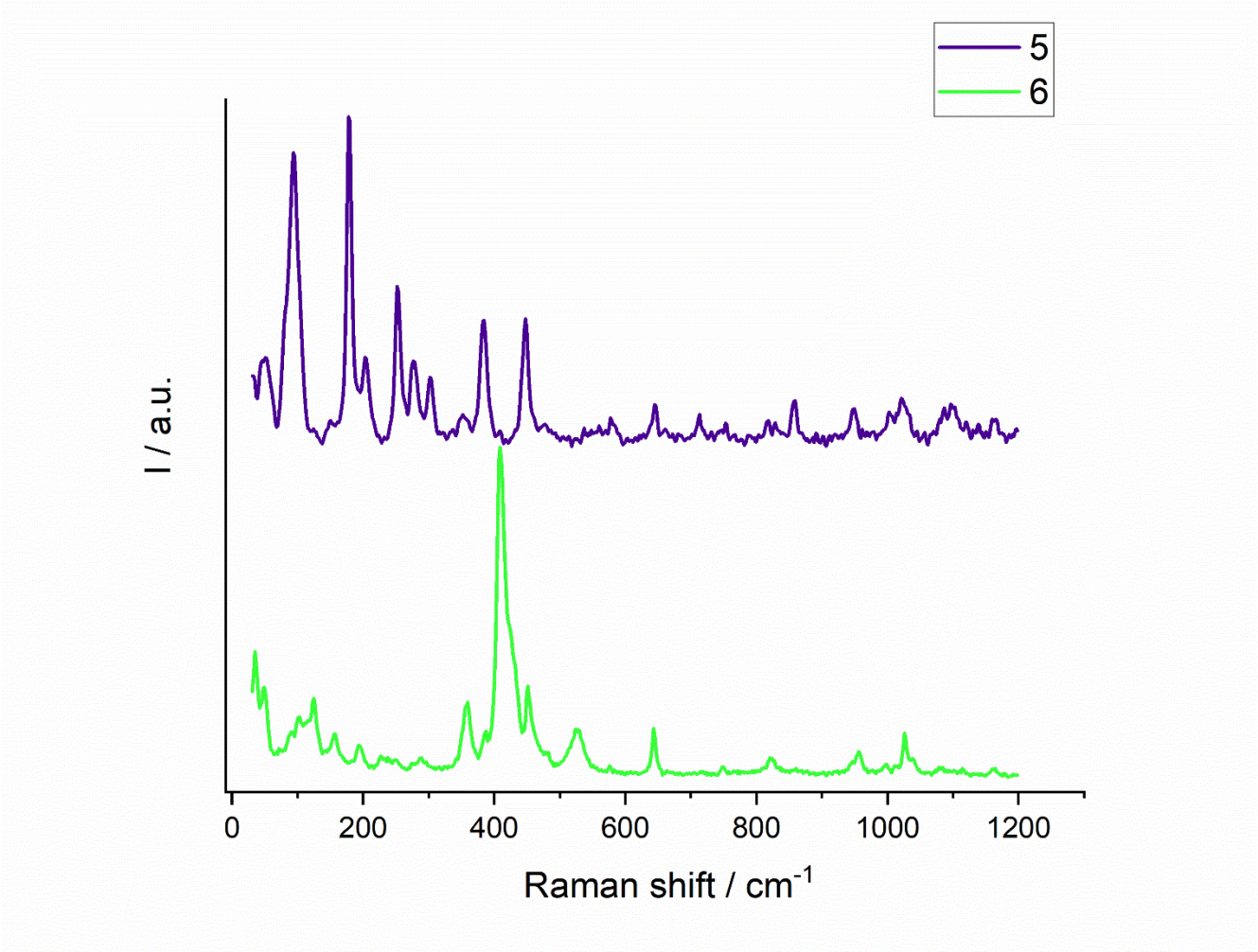

Figure 7. Raman spectra of compound **5** (top purple line, 5) and of dimeric complex **6** (bottom green line, 6).

In the Raman spectra of the starting complex **5**, figure 7, we find the typical **Fe-Br** stretching modes in the region between **200-300 cm^{-1}** [57–59], as expected from its known crystal structure [34]. The striking difference in the spectra of compound **6**, instead, is due to the presence of a very intense band with a maximum at **409 cm^{-1}** assigned to the symmetric stretching of the **Fe-O-Fe** moiety. In comparison with **2**, **3** and **4**, the asymmetric stretching vibration band in the region between **750-900 cm^{-1}** is not present

(see Figure S5); in fact, according to the selection rules, such vibrational mode is forbidden in the Raman spectrum due to the centrosymmetric nature of **6**. Moreover, bands that can be ascribed to Fe-N stretching vibration bands are present in both the precursor **5** and complex **6** at **381 cm^{-1}** and **447 cm^{-1}** [61–63].

Table 2. Raman frequencies (cm^{-1}) and assignment to the corresponding vibrational modes of the compounds under investigation

1	**2**	**3**	**4**	**5**	**6**	Assignment
	849	861	873			ν_{as} (Fe-O-Fe)
				447	451	ν (Fe-N)
	414	378	367		409	ν_s (Fe-O-Fe)
				381		ν (Fe-N)
294				302		
				277		
				252		ν (Fe-Br)
	217	212	217			
203						
	154	158				δ (Fe-O-Fe)
90	92			94		δ (Br-Fe-Br)

3. Conclusions

In conclusion, we have reported here the crystal structure determination of three new μ-oxo bridged iron complexes of the Pyclen family. The steric hindrance of the tetraaza-macrocyclic ligand and the nature of the starting compound are fundamental in determining the structure of the final compound. A centrosymmetric μ-oxo dimer is observed for the less hindered Pyclen ligand **L3**, whilst in the case of the bulkier *p*-^{t}Bu-C_6H_4-CH_2- substituted ligand **L1**, a non-symmetrical dimer is obtained. A very interesting trimer, bridged by a ferrate anion is formed instead when the non-symmetrical μ-oxo bridged complex **4** is treated with organic base. We have shown that Raman spectroscopy especially at low frequencies is perfectly suited to help, together with XRD analysis, in the recognition of the characteristic features of these complexes, revealing the presence of μ-oxo bridges, their symmetry and allowing for interesting information about Fe-X bonds. For instance, the occurrence of the typical pattern of

tetrabromoferrate can be detected by this simple and fast technique. The relevance of those dimers and trimers that, as we have shown, can be easily formed in the presence of even adventitious traces of water (*i.e.* non-distilled solvents) in catalytic oxidation reactions is currently under study in our laboratories.

4. Experimental section

4.1 General considerations

All chemicals and solvents were commercially available and used as received except where specified. ^{1}H NMR analyses were performed with 400 MHz spectrometers at room temperature. The coupling constants (J) are expressed in hertz (Hz), and the chemical shifts (δ) in ppm. Low resolution MS spectra were recorded with instruments equipped with ESI/ion trap sources. The values are expressed as mass − charge ratio and the relative intensities of the most significant peaks are shown in brackets. Elemental analyses were recorded in the analytical laboratories of Università degli Studi di Milano. The ligands **L1** [35], **L2** [28] and **L3** [34], and complexes **1** [35] and **5** [34] were synthesized as already reported.

4.2 XRD analysis and crystal structure determination

Suitable single crystals were selected under an optical microscope, coated with a perfluorinated oil and mounted on glass fiber onto the goniometer head. X-ray diffraction experiments were performed on a Bruker Smart APEX II CCD area-detector diffractometer with graphite monochromated Mo-Kα radiation (λ = 0.71073 Å) in the ω-scan mode at 150 K. The frames were integrated and corrected for Lorentz-polarization effects with the Bruker SAINT software package [64]. The intensity data were then corrected for absorption by using SADABS [65]. No decay correction was applied. The structure was solved by direct methods (SIR-97) [66] and refined by iterative cycles of full-matrix least-squares on Fo^2 and Fourier-difference synthesis with SHELXL-97 [67] within the WinGX interface [68]. Molecular drawings for publication were made with *Mercury* [69]. Crystallographic data for **2**, **4** and **6** were deposited with Cambridge Crystallographic Data Centre with deposition numbers 2175110 (**2**), 2175109 (**4**) and 2175108 (**6**) and can be retrieved free of charge on https://www.ccdc.cam.ac.uk/.

Details on structure refinement and geometrical parameters are given in the Supporting Information.

4.3 Raman spectroscopy

Micro-Raman spectroscopy was carried out using a Horiba LabRam HR evolution at the Dipartimento di Scienze della Terra “A. Desio” of the Università degli Studi di Milano. The spectrometer is equipped

with a Nd-Yag 532 nm/100mW with Ultra Low Frequency (ULF) filters. Scattered light was collected by a 100X objective (NA aperture = 0.9) in backscattering geometry; a diffraction grating with 600 lines/mm and the hole set at 200 μm were used. The spectra have been detected by a Peltier-cooled Charge Couple Detector. To balance signal to noise and to reduce the damage of the highly absorbing samples 3 accumulations for 60 seconds were collected with a laser power set to 0.1%. Instrument calibration was performed before each round of analysis using the peak at 520.70 cm^{-1} of a silicon wafer.

4.4 Synthesis of the complexes

[(L1FeBr)*μ*-O(FeBr$_3$)] (2): 36 mg (0.035mmol) of **[(**L1H$^+$**)]FeBr$_4^-$ (1)** were dissolved in acetonitrile (4 mL) and 10 μL (0.07 mmol) of triethylamine were added. XRD quality dark red prismatic crystals were collected by slow diffusion of diethyl ether. **Elemental analysis:** Calculated for $C_{44}H_{60}Br_4Fe_2N_4O$ C, 48.38; H, 5.54; N, 5.13; Found C, 48.81; H, 6.04; N, 5.24. **ESI-MS(+)** in methanol: 810.35 (**L1**FeBrOMe), 762.67 (**L1**Fe(OMe)$_2$), 731,81 (**L1**FeOMe), 645,97 (**L1**H$^+$).

[(L2FeBr)μ-O(FeBr$_2$)μ-O(FeBrL2)]Br (4): 27 mg (0.026 mmol) of **[(L2FeBr)*μ*-O(FeBr$_3$)] (3)** were dissolved in acetonitrile (4 mL) and 10 μL (0.07 mmol) of triethylamine were added. XRD quality red prismatic crystals were collected by slow diffusion of diethyl ether. **ESI-MS(+)** in methanol: 594.36 (L2Fe(OMe)$_2$), 563.57 (L2FeOMe). Unfortunately, the quantity of obtained crystals was not sufficient to perform a reliable Elemental analysis.

[μ-O(L3FeBr)$_2$]Br$_2$ (6): 18 mg (0.035 mmol) of **[L3FeBr$_2$]Br (5)** were dissolved in 4 mL of acetonitrile and 10 μL (0.07 mmol) of triethylamine were added. XRD quality brown block crystals were collected by slow diffusion of diethyl ether. **Elemental Analysis:** Calculated for $C_{22}H_{36}Br_4Fe_2N_8O$ C, 30.78; H, 4.22; N, 13.03; Found C, 30.05; H, 4.04; N, 12.78. **ESI-MS(+)** in methanol: 572.18 (**L3**Fe(OMe)OFe**L3**), 540.51 (**L3**FeOFe**L3**), 320.24 (**L3**Fe(OMe)$_2$-2H), 260.28 (**L3**Fe-2H).

CRediT authorship contribution statement

Nicola Panza: Conceptualization, Data curation, Writing - original draft, Visualization. **Armando di Biase**: structure determination by single crystal X-Ray Diffraction, Data curation, Writing. **Alessandro Caselli**: Conceptualization, Methodology, Writing - review & editing, Supervision, Project administration, Funding acquisition.

Declaration of Competing Interest

There are no conflicts to declare.

Acknowledgements

We thank the MUR-Italy (Ph.D. fellowships to N. P. and A.d.B.) and the University of Milan (PSR 2020 – financed project ‘‘Catalytic strategies for the synthesis of high added-value molecules from bio-based starting materials’’) for financial support. Prof. Patrizia Fumagalli (Dipartimento di Scienze della Terra “Arditi Desio”, University of Milano) is gratefully acknowledge for her precious help in the collection and analysis of Raman spectra. Prof. Silvia Rizzato (Dipartimento di Chimica, University of Milano) is gratefully acknowledge for helpful discussion on XRD structure refinement.

Appendix A. Supplementary data

Supplementary data associated with this article can be found, in the online version, at: …….

References

[1] R. Solbrig, L.L. Duff, D.F. Shiver, I.M. Klotz, Raman and infrared spectroscopy of the oxo-bridged iron(III) complex, $[Cl_3Fe\text{-}O\text{-}FeCl_3]^{-2}$ as a spectroscopic model for the oxo bridge in hemerythrin and ribonucleotide reductase, J. Inorg. Biochem. 17 (1982) 69–74. https://doi.org/10.1016/S0162-0134(00)80231-7.

[2] J.E. Plowman, M. Loehr, C.K. Schauer, O.P. Anderson, Crystal and molecular structure of the (μ-oxo)bis[aquobis(phenanthroline)iron(III)] complex, a Raman spectroscopic model for the binuclear iron site in hemerythrin and ribonucleotide reductase, Inorg. Chem. 23 (1984) 3553–3559. https://doi.org/10.1021/ic00190a024

[3] A.K. Shiemke, T.M. Loehr, J. Sanders-Loehr, Resonance Raman study of the .mu.-oxo-bridged binuclear iron center in oxyhemerythrin, J. Am. Chem. Soc. 106 (1984) 4951–4956. https://doi.org/10.1021/ja00329a054.

[4] J. Sanders-Loehr, W.D. Wheeler, A.K. Shiemke, B.A. Averill, T.M. Loehr, Electronic and Raman spectroscopic properties of oxo-bridged dinuclear iron centers in proteins and model compounds, J. Am. Chem. Soc. 111 (1989) 8084–8093. https://doi.org/10.1021/ja00203a003.

[5] P. Gomez-Romero, E.H. Witten, W.M. Reiff, G. Backes, J. Sanders-Loehr, G.B. Jameson, Dissymmetry effects in .mu.-oxo diiron(III) species: structures and spectroscopic properties of [N5FeOFeX3]+ (X = Cl, Br) and implications for oxo-bridged dinuclear iron proteins, J. Am. Chem. Soc. 111 (1989) 9039–9047. https://doi.org/10.1021/ja00207a009.

[6] B.G. Fox, J. Shanklin, J. Ai, T.M. Loehr, J. Sanders-Loehr, Resonance Raman Evidence for an Fe-O-Fe Center in Stearoyl-ACP Desaturase. Primary Sequence Identity with Other Diiron-Oxo Proteins, Biochemistry 33 (1994) 12776–12786. https://doi.org/10.1021/bi00209a008.

[7] D.M. Kurtz, Oxo- and hydroxo-bridged diiron complexes: a chemical perspective on a biological unit, Chem. Rev. 90 (1990) 585–606. https://doi.org/10.1021/cr00102a002.

[8] S.K. Dutta, R. Werner, U. Flörke, S. Mohanta, K.K. Nanda, W. Haase, K. Nag, Model Compounds for Iron Proteins. Structures and Magnetic, Spectroscopic, and Redox Properties of $Fe^{III}M^{II}$ and $[Co^{III}Fe^{III}]_2O$ Complexes with (μ-Carboxylato)bis(μ-phenoxo)dimetalate and (μ-Oxo)diiron(III) Cores, Inorg. Chem. 35 (1996) 2292–2300. https://doi.org/10.1021/ic9508334.

[9] S. Kumar, S. Vaidya, M. Pissas, Y. Sanakis, R. Gupta, Synthesis and Properties of Dinuclear μ-Oxodiiron(III) Complexes of Amide-Based Macrocyclic Ligands, Eur. J. Inorg. Chem. 2012 (2012) 5525–5533. https://doi.org/10.1002/ejic.201200683.

[10] J.B.H. Strautmann, S. Dammers, T. Limpke, J. Parthier, T.P. Zimmermann, S. Walleck, G. Heinze-Brückner, A. Stammler, H. Bögge, T. Glaser, Design and synthesis of a dinucleating ligand system with varying terminal donor functions that provides no bridging donor and its application to the synthesis of a series of Fe^{III}-μ-O-Fe^{III} complexes, Dalton Trans. 45 (2016) 3340–3361. https://doi.org/10.1039/c5dt03711e.

[11] M.C. Esmelindro, E.G. Oestreicher, H. Márquez-Alvarez, C. Dariva, S.M.S. Egues, C. Fernandes, A.J. Bortoluzzi, V. Drago, O.A.C. Antunes, Catalytic oxidation of cyclohexane by a binuclear Fe(III) complex

biomimetic to methane monooxygenase, J. Inorg. Biochem. 99 (2005) 2054–2061. https://doi.org/10.1016/j.jinorgbio.2005.07.007.

[12] A. Kejriwal, A.N. Biswas, A. Choudhury, P. Bandyopadhyay, Diferric oxo-bridged complexes of a polydentate aminopyridyl ligand: Synthesis, structure and catalytic reactivity, Transition Met. Chem. 39 (2014) 909–915. https://doi.org/10.1007/s11243-014-9875-0.

[13] Y. Sakaguchi, A. Call, M. Cibian, K. Yamauchi, K. Sakai, An earth-abundant system for light-driven CO_2 reduction to CO using a pyridinophane iron catalyst, Chem. Commun. 55 (2019) 8552–8555. https://doi.org/10.1039/C9CC04191E.

[14] W. Lin, L. Zhang, H. Suo, A. Vignesh, N. Yousuf, X. Hao, W.H. Sun, Synthesis of characteristic polyisoprenes using rationally designed iminopyridyl metal (Fe and Co) precatalysts: Investigation of co-catalysts and steric influence on their catalytic activity, New J. Chem. 44 (2020) 8076–8084. https://doi.org/10.1039/d0nj00942c.

[15] N. Raffard, V. Balland, J. Simaan, S. Létard, M. Nierlich, K. Miki, F. Banse, E. Anxolabéhère-Mallart, J.-J. Girerd, Bio-inspired iron catalysts for degradation of aromatic pollutants and alkane hydroxylation, C. R. Chim. 5 (2002) 99–109. https://doi.org/10.1016/S1631-0748(02)01359-0.

[16] S. Taktak, S. V. Kryatov, T.E. Haas, E. V. Rybak-Akimova, Diiron(III) oxo-bridged complexes with BPMEN and additional monodentate or bidentate ligands: Synthesis and reactivity in olefin epoxidation with H_2O_2, J. Mol. Catal. A: Chem. 259 (2006) 24–34. https://doi.org/10.1016/j.molcata.2006.05.071.

[17] S.M. Brewer, T.M. Schwartz, M.A. Mekhail, L.S. Turan, T.J. Prior, T.J. Hubin, B.G. Janesko, K.N. Green, Mechanistic Insights into Iron-Catalyzed C-H Bond Activation and C-C Coupling, Organometallics 40 (2021) 2467–2477. https://doi.org/10.1021/acs.organomet.1c00211.

[18] A. Caselli, F. Cesana, E. Gallo, N. Casati, P. Macchi, M. Sisti, G. Celentano, S. Cenini, Designing new ligands: asymmetric cyclopropanation by Cu(I) complexes based on functionalised pyridine-containing macrocyclic ligands, Dalton Trans. (2008) 4202–4205. https://doi.org/10.1039/B809317M.

[19] B. Castano, E. Gallo, D.J. Cole-Hamilton, V. Dal Santo, R. Psaro, A. Caselli, Continuous flow asymmetric cyclopropanation reactions using Cu(I) complexes of Pc-L* ligands supported on silica as catalysts with carbon dioxide as a carrier, Green Chem. 16 (2014) 3202–3209. https://doi.org/10.1039/c4gc00119b.

[20] T. Pedrazzini, P. Pirovano, M. Dell'Acqua, F. Ragaini, P. Illiano, P. Macchi, G. Abbiati, A. Caselli, Organometallic Reactivity of [Silver(I)(Pyridine-Containing Ligand)] Complexes Relevant to Catalysis, Eur. J. Inorg. Chem. 2015 (2015) 5089–5098. https://doi.org/10.1002/ejic.201500771.

[21] G. Tseberlidis, A. Caselli, R. Vicente, Carbene X-H bond insertions catalyzed by copper(I) macrocyclic pyridine-containing ligand (PcL) complexes, J. Organomet. Chem. 835 (2017) 1–5. https://doi.org/10.1016/j.jorganchem.2017.02.027.

[22] V. Pirovano, A. Caselli, A. Colombo, C. Dragonetti, M. Giannangeli, E. Rossi, E. Brambilla, Synthesis of 2-alkenylidene-3-oxoindolines: cascade reactions of 4H-furo [3,2-b]indoles with diazoacetates catalyzed by a Cu(I) macrocyclic pyridine-containing ligand (PcL) complex, ChemCatChem. 12 (2020) 5250–5255. https://doi.org/10.1002/cctc.202000887.

[23] V. Pirovano, G. Hamdan, D. Garanzini, E. Brambilla, E. Rossi, A. Caselli, G. Abbiati, [Ag(PcL)]-Catalyzed Domino Reactions of 2-Alkynylbenzaldehydes with Electron-Poor Anilines: Synthesis of 1-Aminoisochromenes, Eur. J. Org. Chem. 2020 (2020) 2592–2599. https://doi.org/10.1002/ejoc.202000275.

[24] M. Cavalleri, N. Panza, A. Biase, G. Tseberlidis, S. Rizzato, G. Abbiati, A. Caselli, [Zinc(II)(Pyridine-Containing Ligand)] Complexes as Single-Component Efficient Catalyst for Chemical Fixation of CO_2 with Epoxides , Eur. J. Org. Chem. 2021 (2021) 2764–2771. https://doi.org/10.1002/ejoc.202100409.

[25] N. Panza, G. Tseberlidis, A. Caselli, R. Vicente, Recent progresses in the chemistry of 12-membered pyridine-containing tetraazamacrocycles: From synthesis to catalysis, Dalton Trans. (2022). https://doi.org/10.1039/d2dt00597b.

[26] H.M. Johnston, D.M. Freire, C. Mantsorov, N. Jamison, K.N. Green, Manganese (III/IV) μ-Oxo Dimers and Manganese (III) Monomers with Tetraaza Macrocyclic Ligands and Historically Relevant Open-Chain Ligands, Eur. J. Inorg. Chem. (2022). https://doi.org/10.1002/EJIC.202200039.

[27] G. Tseberlidis, D. Intrieri, A. Caselli, Catalytic Applications of Pyridine-Containing Macrocyclic Complexes, Eur. J. Inorg. Chem. 2017 (2017) 3589–3603. https://doi.org/10.1002/ejic.201700633.

[28] G. Tseberlidis, L. Demonti, V. Pirovano, M. Scavini, S. Cappelli, S. Rizzato, R. Vicente, A. Caselli, Controlling Selectivity in Alkene Oxidation: Anion Driven Epoxidation or Dihydroxylation Catalysed by [Iron(III)(Pyridine-Containing Ligand)] Complexes, ChemCatChem 11 (2019) 4907–4915. https://doi.org/10.1002/cctc.201901045.

[29] J. Serrano-Plana, W.N. Oloo, L. Acosta-Rueda, K.K. Meier, B. Verdejo, E. García-España, M.G. Basallote, E. Münck, L. Que, A. Company, M. Costas, Trapping a Highly Reactive Nonheme Iron Intermediate That Oxygenates Strong C—H Bonds with Stereoretention, J. Am. Chem. Soc. 137 (2015) 15833–15842. https://doi.org/10.1021/jacs.5b09904.

[30] W.N. Oloo, R. Banerjee, J.D. Lipscomb, L. Que, Equilibrating (L)Fe^{III}-OOAc and (L)Fe^{V}(O) Species in Hydrocarbon Oxidations by Bio-Inspired Nonheme Iron Catalysts Using H_2O_2 and AcOH, J. Am. Chem. Soc. 139 (2017) 17313–17326. https://doi.org/10.1021/jacs.7b06246.

[31] R. Fan, J. Serrano-Plana, W.N. Oloo, A. Draksharapu, E. Delgado-Pinar, A. Company, V. Martin-Diaconescu, M. Borrell, J. Lloret-Fillol, E. Garcia-Espana, Y. Guo, E.L. Bominaar, L. Que Jr., M. Costas, E. Munck, Spectroscopic and DFT Characterization of a Highly Reactive Nonheme Fe(V)-Oxo Intermediate, J. Am. Chem. Soc. 140 (2018) 3916–3928. https://doi.org/10.1021/jacs.7b11400.

[32] J. Serrano-Plana, F. Acuña-Parés, V. Dantignana, W.N. Oloo, E. Castillo, A. Draksharapu, C.J. Whiteoak, V. Martin-Diaconescu, M.G. Basallote, J.M. Luis, L. Que Jr., M. Costas, A. Company, Acid-Triggered O−O Bond Heterolysis of a Nonheme Fe^{III}(OOH) Species for the Stereospecific Hydroxylation of Strong C−H Bonds, Chem. Eur. J. 24 (2018) 5331–5340. https://doi.org/10.1002/chem.201704851.

[33] V. Dantignana, J. Serrano-Plana, A. Draksharapu, C. Magallón, S. Banerjee, R. Fan, I. Gamba, Y. Guo, L. Que, M. Costas, A. Company, Spectroscopic and Reactivity Comparisons between Nonheme Oxoiron(IV) and Oxoiron(V) Species Bearing the Same Ancillary Ligand, J. Am. Chem. Soc. 141 (2019) 15078–15091. https://doi.org/10.1021/jacs.9b05758.

[34] N. Panza, A. Biase, S. Rizzato, E. Gallo, G. Tseberlidis, A. Caselli, Catalytic Selective Oxidation of Primary and Secondary Alcohols Using Nonheme [Iron(III)(Pyridine-Containing Ligand)] Complexes, Eur. J. Org. Chem. 2020 (2020) 6635–6644. https://doi.org/10.1002/ejoc.202001201.

[35] N. Panza, A. di Biase, E. Gallo, A. Caselli, Unexpected "ferrate" species as single-component catalyst for the cycloaddition of CO_2 to epoxides, J. CO2 Util. 51 (2021) 101635. https://doi.org/10.1016/j.jcou.2021.101635.

[36] L. Benhamou, H. Jaafar, A. Thibon, M. Lachkar, D. Mandon, Asymmetry and steric hindrance in tripodal ligands: Reaching the limit for octahedral geometry with the newly synthesized [(6-bromo 2-pyridylmethyl) (6-fluoro 2-pyridylmethyl) (2-pyridylmethyl)] amine tripod in $FeCl_2$ complexes, Inorganica Chim. Acta 373 (2011) 195–200. https://doi.org/10.1016/j.ica.2011.04.015.

[37] Y. Yang, C. Lu, H. Wang, X. Liu, Amide bond cleavage initiated by coordination with transition metal ions and tuned by an auxiliary ligand, Dalton Transactions. 45 (2016) 10289–10296. https://doi.org/10.1039/c6dt01411a.

[38] N.K. Thallaj, O. Rotthaus, L. Benhamou, N. Humbert, M. Elhabiri, M. Lachkar, R. Welter, A.-M. Albrecht-Gary, D. Mandon, Reactivity of Molecular Dioxygen towards a Series of Isostructural Dichloroiron(III) Complexes with Tripodal Tetraamine Ligands: General Access to μ-Oxodiiron(III) Complexes and Effect of α-Fluorination on the Reaction Kinetics, Chem. Eur. J. 14 (2008) 6742–6753. https://doi.org/10.1002/chem.200701967.

[39] N. Raffard-Pons Y Moll, F. Banse, K. Miki, M. Nierlich, J.J. Girerd, Hydroxylation of hexane using dioxygen and trimethylhydroquinone: Biomimetic catalysis by an unsymmetrical diiron-μ-oxo complex, Eur. J. Inorg. Chem. (2002) 1941–1944. https://doi.org/10.1002/1099-0682(200208)2002:8<1941::AID-EJIC1941>3.0.CO;2-B.

[40] V. Félix, J. Costa, R. Delgado, M.G.B. Drew, M.T. Duarte, C. Resende, X-Ray diffraction and molecular mechanics studies of 12-, 13-, and 14-membered tetraaza macrocycles containing pyridine: Effect of the macrocyclic cavity size on the selectivity of the metal ion, J. Chem. Soc., Dalton Trans. (2001) 1462–1471. https://doi.org/10.1039/b009773j.

[41] Complex **3** was synthetized directly from **L2**: **L2** (0.5 mmol, 290 mg) was dissolved in acetonitrile (10 mL and $FeBr_3$ (1 mmol, 295 mg) in acetonitrile (5 mL) was slowly added. The reaction was stirred for 3 h at 40 °C and the product separated by filtration as a dark red solid (370 mg, 80%). **Elemental analysis:** Calculated for $C_{32}H_{36}Br_4Fe_2N_4O$ C, 41.60; H, 3.93; N, 6.06; found C, 40.88; H, 3.87; N, 6.14. **ESI-MS(+)** in methanol: 642.17 (**L2**FeBrOMe), 594.17 (**L2**Fe$(OMe)_2$)

[42] N. Arulsamy, D.J. Hodgson, J. Glerup, Mononuclear and binuclear oxo-bridged iron(III) complexes of N,N′-bis(2-pyridylmethyl)ethane-1,2-diamine (bispicen), Inorganica Chim. Acta 209 (1993) 61–69. https://doi.org/10.1016/S0020-1693(00)84981-6.

[43] T. Kojima, R.A. Leising, S. Yan, L. Que, Alkane functionalization at nonheme iron centers. Stoichiometric transfer of metal-bound ligands to alkane, J. Am. Chem. Soc. 115 (1993) 11328–11335. https://doi.org/10.1021/ja00077a035.

[44] R.M. Buchanan, R.J. O'Brien, J.F. Richardson, J.-M. Latour, Synthesis and properties of a binuclear (μ-oxo) diiron(III) complex containing a tripodal polybenzimidazole ligand, Inorganica Chim. Acta 214 (1993) 33–40. https://doi.org/https://doi.org/10.1016/S0020-1693(00)87523-4.

[45] M. Pascaly, M. Duda, A. Rompel, B.H. Sift, W. Meyer-Klaucke, B. Krebs, Novel iron(III) complexes with imidazole containing tripodal ligands as model systems for catechol dioxygenases, Inorganica Chimica Acta. 291 (1999) 289–299. https://doi.org/https://doi.org/10.1016/S0020-1693(99)00129-2.

[46] B. Kwak, K. Woong Cho, M. Pyo, M. Soo Lah, Synthesis and characterization of a ferric complex of the tripodal ligand tris(2-benzimidazolylmethyl)amine—a superoxide dismutase mimic, Inorganica Chimica Acta. 290 (1999) 21–27. https://doi.org/https://doi.org/10.1016/S0020-1693(99)00091-2.

[47] M. Merkel, M. Pascaly, B. Krebs, J. Astner, S.P. Foxon, S. Schindler, Chelate ring size variations and their effects on coordination chemistry and catechol dioxygenase reactivity of iron(III) complexes, Inorg. Chem. 44 (2005) 7582–7589. https://doi.org/10.1021/ic050708k.

[48] E.A. Duban, T.N. Drebushchak, K.P. Bryliakov, E.P. Talsi, X-ray crystal structure of [BPMEN(Cl)$Fe^{III}OFe^{III}$(Cl)BPMEN]$(ClO_4)_2$ [BPMEN = N,N'-dimethyl-N,N'-bis(2-pyridylmethyl)ethane-1,2-diamine] and the assignment of its ^{1}H NMR peaks in CD_3CN, Mendeleev Commun. 17 (2007) 291–293. https://doi.org/https://doi.org/10.1016/j.mencom.2007.09.015.

[49] H. Sun, M. Wang, F. Li, P. Li, Z. Zhao, L. Sun, Synthesis and structure of a μ-oxo diiron(III) complex with an N-pyridylmethyl-N,N-bis(4-methylbenzimidazol-2-yl)amine ligand and its catalytic property for hydrocarbon oxidation, App. Organomet. Chem. 22 (2008) 573–576. https://doi.org/https://doi.org/10.1002/aoc.1444.

[50] C. Wegeberg, A. de Aguirre, F. Maseras, C.J. McKenzie, Photosynthesis of a Dihydroimidazopyridine Chelate Shines Light on the Reactions of a Photoactivated Iron(III) Complex with O_2, Inorg. Chem. 59 (2020) 16281–16290. https://doi.org/10.1021/acs.inorgchem.0c02063.

[51] C. Brémard, P. Kowalewski, J.C. Merlin, S. Moreau, Resonance Raman enhancement of the oxo-bridged dinuclear iron center: Vibrational modes in iron(III) physiological-type porphyrin complexes, J. Raman Spectrosc. 23 (1992) 325–333. https://doi.org/10.1002/jrs.1250230603.

[52] I.M. Wasser, C.F. Martens, C.N. Verani, E. Rentschler, H.W. Huang, P. Moënne-Loccoz, L.N. Zakharov, A.L. Rheingold, K.D. Karlin, Synthesis and Spectroscopy of μ-Oxo (O^{2-})-Bridged Heme/Non-heme Diiron Complexes: Models for the Active Site of Nitric Oxide Reductase, Inorg. Chem. 43 (2004) 651–662. https://doi.org/10.1021/ic0348143.

[53] T. Mejean, M.T. Forel, M.T. Bourgeois, M. Jacon, Resonance Raman spectra of $FeBr_4^-$ in various solvents and excited in the $^4A_1$ ^4E *d–d* band, J. Chem. Phys. 72 (1980) 687–693. https://doi.org/10.1063/1.438903.

[54] G.P. Bhavsar, K. Sathianandan, Vibrational analysis of tetrahaloferrates of the type $FeCl_{4-n}Br^{-1}{}_n$, J. Mol. Struct. 16 (1973) 343–345. https://doi.org/10.1016/0022-2860(73)80075-4

[55] J.R. Schoonover, J.F. Ni, L. Roecker, P.S. White, T.J. Meyer, Structural and Resonance Raman Studies of an Oxygen-Evolving Catalyst. Crystal Structure of [$(bpy)_2(H_2O)Ru^{III}ORu^{IV}(OH)(bpy)_2$]$(ClO_4)_4$, Inorg. Chem. 35 (1996) 5885–5892. https://doi.org/10.1021/ic960348o.

[56] G. Haselhorst, K. Wieghardt, S. Keller, B. Schrader, The (.mu.-oxo)bis[trichloroferrate(III)] dianion revisited, Inorg. Chem. 32 (1993) 520–525. https://doi.org/10.1021/ic00057a006.

[57] C.A. Clausen, M.L. Good, Moessbauer and far-infrared studies of tetrahaloferrate anions of the type FeCl4-nBrn-, Inorg. Chem. 9 (1970) 220–223. https://doi.org/10.1021/ic50084a005.

[58] T. Birchall, M.F. Morris, Mössbauer and Infrared Spectra of Tetrahedral Complexes of Iron(II) Halides with Thioamides and Related Ligands, Can. J. Chem. 50 (1972) 211–216. https://doi.org/10.1139/v72-031.

[59] N.T. Madhu, P.K. Radhakrishnan, M. Grunert, P. Weinberger, W. Linert, Synthesis and thermal studies on iron(III) complexes of 4-N-(4′-antipyrylmethylidene)aminoantipyrine with varying counter ions, Thermochim. Acta 407 (2003) 73–84. https://doi.org/10.1016/S0040-6031(03)00309-5.

[60] R.E. Norman, S. Yan, L. Que, G. Backes, J. Ling, J. Sanders-Loehr, J.H. Zhang, C.J. O'Connor, (.mu.-Oxo)(.mu.-carboxylato)diiron(III) complexes with distinct iron sites. Consequences of the inequivalence and its relevance to dinuclear iron-oxo proteins, J. Am. Chem. Soc. 112 (1990) 1554–1562. https://doi.org/10.1021/ja00160a039.

[61] B. Huchinson, M. Hoffbauer, J. Takemoto, Low-frequency i.r. spectral assignments for transition metal poly(1-pyrazoyl)borate complexes, Spectrochim. Acta A: Mol. Spectrosc. 32 (1976) 1785–1792. https://doi.org/10.1016/0584-8539(76)80230-9.

[62] W.S. Szulbinski, R.S. Czernuszewicz, The effect of ligand structure on surface enhanced Raman scattering by Fe(II) macrocyclic complexes: $[Fe^{II}TPC]^{2+}$ and $[Fe^{II}DPC]^{2+}$, Inorganica Chim. Acta 247 (1996) 11–18. https://doi.org/10.1016/0020-1693(95)04946-0.

[63] C.C. Wagner, E.J. Baran, Vibrational spectra of two Fe(III)/EDTA complexes useful for iron supplementation, Spectrochim. Acta A: Mol. Biomol. Spectrosc. 75 (2010) 807–810. https://doi.org/10.1016/j.saa.2009.11.059.

[64] Bruker AXS Inc., SAINT, (2007).

[65] Bruker AXS Inc., SADABS Area-Detector Absorption Correction Program, (2001).

[66] A. Altomare, M.C. Burla, M. Camalli, G.L. Cascarano, C. Giacovazzo, A. Guagliardi, A.G.G. Moliterni, G. Polidori, R. Spagna, SIR 97: a new tool for crystal structure determination and refinement, J. Appl. Crystallogr. 32 (1999) 115–119. https://doi.org/10.1107/S0021889898007717.

[67] G.M. Sheldrick, Crystal structure refinement with SHELXL, Acta Cryst. C Struct. Chem. C71 (2015) 3–8. https://doi.org/10.1107/S2053229614024218.

[68] L.J. Farrugia, WinGX suite for small-molecule single-crystal crystallography, J. Appl. Crystallogr. 32 (1999) 837–838. https://doi.org/10.1107/S0021889899006020.

[69] C.F. MacRae, I. Sovago, S.J. Cottrell, P.T.A. Galek, P. McCabe, E. Pidcock, M. Platings, G.P. Shields, J.S. Stevens, M. Towler, P.A. Wood, Mercury 4.0: From visualization to analysis, design and prediction, J. Appl. Crystallogr. 53 (2020) 226–235. https://doi.org/10.1107/S1600576719014092.